Skeleton Matching with Applications in Severe Weather Detection

Mohammad Mahdi Kamani[a,*], Farshid Farhat[a], Stephen Wistar[b], James Z. Wang[a]

[a]The Pennsylvania State University, University Park, Pennsylvania, USA
[b]Accuweather Inc., State College, Pennsylvania, USA

Abstract

Severe weather conditions cause an enormous amount of damages around the globe. Bow echo patterns in radar images are associated with a number of these destructive conditions such as damaging winds, hail, thunderstorms, and tornadoes. They are detected manually by meteorologists. In this paper, we propose an automatic framework to detect these patterns with high accuracy by introducing novel skeletonization and shape matching approaches. In this framework, first we extract regions with high probability of occurring bow echo from radar images and apply our skeletonization method to extract the skeleton of those regions. Next, we prune these skeletons using our innovative pruning scheme with fuzzy logic. Then, using our proposed shape descriptor, *Skeleton Context*, we can extract bow echo features from these skeletons in order to use them in shape matching algorithm and classification step. The output of classification indicates whether these regions are bow echo with over 97% accuracy.

Keywords: Radar image, severe weather forecasting, skeleton pruning, fuzzy logic, big data analytics

1. Introduction

Monitoring and storing climatic data around the globe provide a vast amount of data for weather condition analysis. In spite of the fact that computational power is emerging continuously, automatic severe weather forecasting is costly and not always accurate. Meteorologists leverage various and complex models to forecast storms using data from a collection of sensors, including tools and data at the Storm Prediction Center (SPC) of the National Oceanic and Atmospheric Administration (NOAA). The data gathered from these sensors are stored historically; hence it can be leveraged to extract historical patterns of different severe weather conditions. Although meteorologists have developed numerous and complicated models for forecasting storms, they still rely significantly on their interpretations instead of automated algorithms. Further, the majority of these models depend on initial conditions and are highly sensitive to noise, making forecasting difficult. Therefore, it is inevitable for this field to combine big data, computer vision, and data mining algorithms with these models to seek faster, more robust, and more accurate results.

Severe weather conditions consist of thunderstorms, tornadoes, floods, lightning, hail, and strong winds. Each of these conditions are investigated widely in meteorological literature, and they need different sources for detection and forecasting, such as satellite images, radar images, temperature, air pressure and wind speed, to name but a few. These events are the primary causes of a large amount of damage around the globe. For instance, according to the *National Severe Storms Laboratory (NSSL)*, damaging winds or *straight-line winds* are the major causes of nearly half of all reports of severe weather conditions in the United States. These winds can reach the speed of 100 miles per hour and have a damage path up to hundreds of miles. Bow echoes, convective line segments with an archery bow shape, are mainly associated with these strong straight-line winds. In some cases, parts of bow echoes can form tornadoes and new thunderstorms. Hence, bow echo detection can be used as a way of forecasting such destructive severe weather conditions. Accurate and on-time forecasting of these events seems necessary and would help to mitigate damages.

As Klimowski *et al.* [1] found 273 cases of bow echoes between 1996 and 2002, it seems popular among weather patterns. Their investigations revealed that bow echoes are causing nearly 33% of severe convectively generated winds in the U.S. [2]. NSSL in partnership with other organizations performed a field experiment on bow echoes called *Bow Echo and Mesoscale Convective Vortex Experiment (BAMEX)* to investigate bow echoes and extremely damaging surface winds with them in more detail [3]. Although, meteorologists have done lots of research on bow echoes and their effects [2, 1, 3, 4], there is no evidence of computer-aided algorithms in bow echo detection and forecasting in the literature. While there is no machine learning and computer vision frameworks for detecting bow echoes, there has been some studies investigating severe weather conditions using satellite images or other tools. Zhou *et al.* [5] build a framework to estimate cloud motions on satellite images especially on hurricanes when clouds form a cyclic or comma shape. Zhang *et al.* [6, 7] use optical flow algorithms [8] on satellite images to predict the location of thunderstorms. However, radar images are different from satellite images in nature representing different information. Hence, the approach to extract a pattern in one of them is not necessarily applicable to the other. Narasimhan and Nayar [9] model se-

vere weather conditions and their effect on the quality of urban images and videos and how to restore them using the structure and depth discontinuities in the scene. The main difference of this research from ours is that the radar images do not have the notion of depth in their images and the structure of the whole image would change during the time. Quinan and Meyer [10] build a system to visualize ensemble of forecasts for meteorologists using an open source platform. Additionally, the shorter abstract of this paper is printed in [11].

In this paper we propose a new method for detecting bow echoes in radar images. This bow shape signature of bow echo leads us to use computer vision algorithms for particular shape detection and matching. In this regard, we first use radar images and develop our algorithm for skeletonization, which then can be used in the shape matching algorithm through our suggested descriptor, *Skeleton Context*. Finally, we use *Mixture Discriminant Analysis (MDA)* to classify bow echo shapes in radar images. Our **contributions** through this research are as follows:

- Introducing a new skeletonization scheme and some criteria for ranking of edges in a skeleton.

- Proposing a novel fuzzy logic based approach for *skeleton pruning*, which is based on inference systems that are closely related to the human inference system. The process is flexible due to the suggested *branch tolerance* window. We introduce two fuzzy transformations of skeletons in the course of pruning them, that is, *Main Skeleton Degree of Belief*, and *Branch Degree of Belief*.

- Introducing a new shape descriptor, based on skeleton samples of a shape, called *skeleton context*. Applying a novel approach on shape matching algorithm, in order to allow *partial shape matching*.

2. Bow Echo Feature Extraction

2.1. Overview

Severe weather conditions such as thunderstorms, tornadoes, hail, and especially strong straight-line winds are associated with bow echoes. The wind with a bow echo can be fierce and reach violent intensity.

The term bow echo was coined by Fujita [12], to describe strong outflow winds associated with storms that spread out in straight lines over the ground. Przybylinski categorize bow echoes in two categories [4]:

- Bow echo patterns associated with derechoes or straight-line winds.

- Bow echo patterns associated with vortices, including tornadoes,

Klimowski *et al.* [1] classify different types of bow echoes and their evolution from meteorologists' point of view. They start with a radar echo and then evolve into a bow echo. In this research, we aim to use this topological feature of these phenomena to detect them using computational approaches.

Our proposed scheme for detecting bow echoes, shown in Figure 1, consists of two main steps, skeleton extraction and matching. In the first step, we take a radar image and extract its regions of interest (parts that we can find bow echoes). Then using our skeletonization and skeleton pruning framework, to extract their skeleton. In the second step, using our suggested shape descriptor, skeleton context, to extract features for shape matching part. After matching those parts to a bow echo prototype, based on the distance between them and their matched bow echo prototype, we are able to identify whether they are a bow echo or not.

2.2. Radar Images and Regions of Interest

Our dataset consists of images from NEXRAD level III radar of National Weather Service (technical name WSR-88D), which can measure precipitation and wind movement in the atmosphere. These images are gathered from 160 active high resolution radar sites around the U.S. continent. We use base reflectivity images from NEXRAD level III radar, which represent the amount of returned power to the radar from transmitted signal after hitting precipitation in the atmosphere. The images have 4-bit color map with $6,000 \times 2,600$ pixels of spatial resolution, which are stored every five minutes [13]. That is, in a whole year there are more than $105,000$ images with mentioned quality. The color map associated to these radar images is shown in Figure 2 having the range from 0 dBZ to 75 dBZ for reflectivity. The range of the reflectivity from 0 dBZ to -30 dBZ, alongside with "No Data" regions (due to spots with beam blockage in the mountains and outside of the U.S.) is represented by a black color.

Bow echoes can be spotted in heavy precipitation red regions on radar images (*i.e.*, with reflectivity of higher than 50 dBZ). As shown in Figure 2, the bow echo happened on May 2 in 2008 over Kansas City. Hence, in searching for bow echoes in radar images, regions of interest are red in color (> 50 dBZ). To extract these parts we can set a threshold on their RGB values, but it would result in patchy areas and not connected regions. Although human eyes can cluster them as a unified region, computer algorithms need to perform a pre-processing in order to connect those parts together. We use some morphological operations such as image closing along with active contours to improve the extraction of the connected components.

2.3. Skeletonization

Skeleton of a shape is a low-level representation that can be used for matching and recognition purposes in various fields of study including image retrieval and shape matching [14] or human pose estimation and recovery [15]. Skeleton can provide a good abstraction of a shape, which contains topological structure and its features. Because it is the simplest representation of a shape, there has been an extensive effort among researchers to develop generic algorithms for skeletonization of shapes [16, 17, 18, 19, 20]. However, Saha *et al.* [21] claim that since there is no "true" skeleton defined for an object, the literature in skeletonization lack of a robust evaluation. The vast majority of the algorithms are based on Blum's "Grassfire"
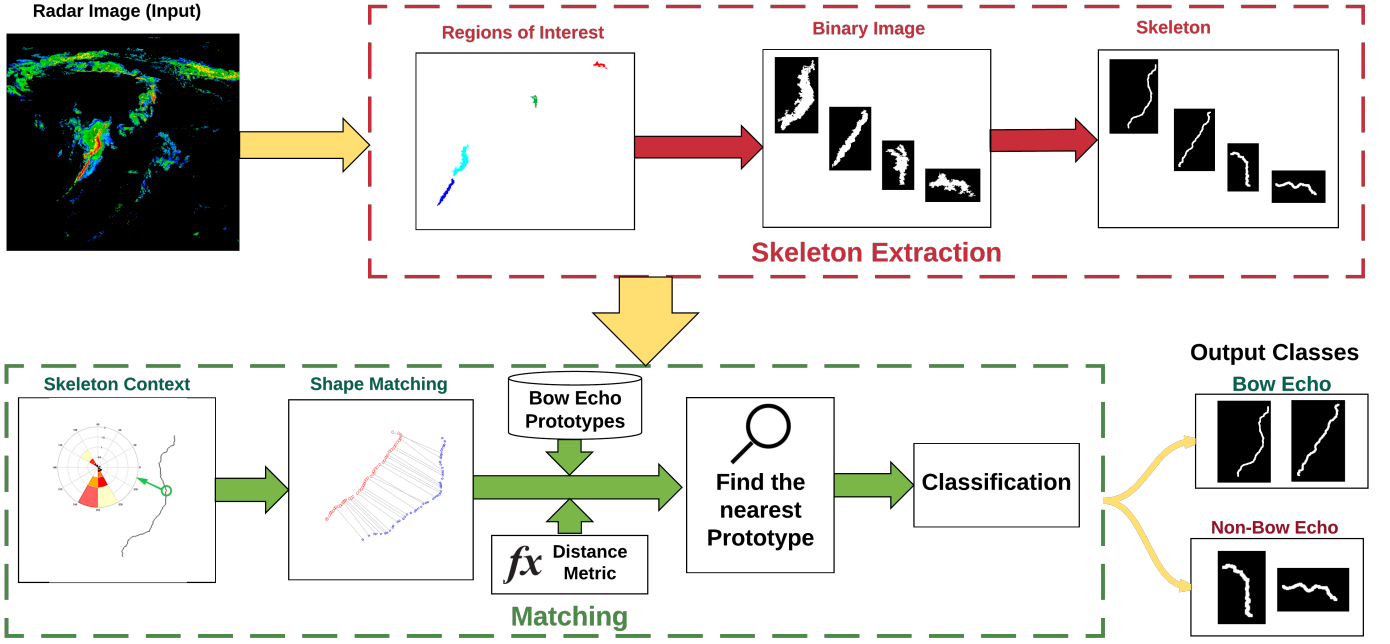
Figure 1: The complete scheme for automatic bow echo detection. In the first stage, it extracts regions of interest, which are red parts in radar images. Then in the skeletonization step, it extracts skeleton map of each part, and prunes it using the proposed algorithm. After finding pruned skeleton, it computes skeleton context and finds the nearest match in the database of bow echo prototypes. Finally, it uses mixture discriminant analysis classifier to detect whether it is a bow echo or not.
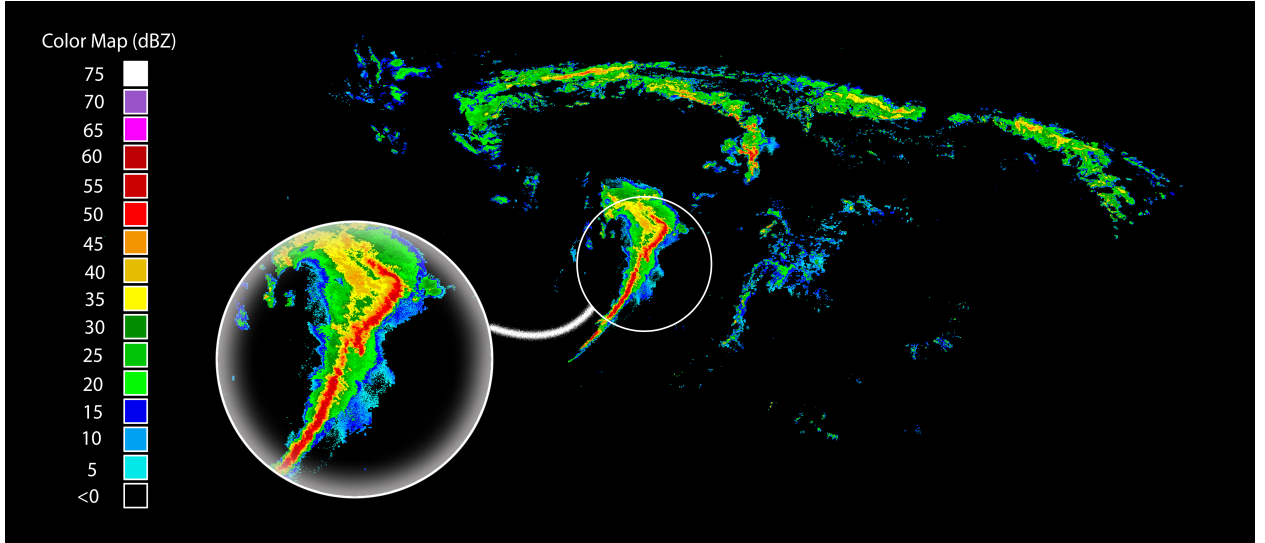

Figure 2: Radar image of the United States Continent with a bow echo, May 2, 2008, 07:10 GMT. We magnify the part that bow echo happened (*i.e.* red regions).

analogy and formulation for skeletonization [22]. The most important key factor in skeletonization algorithms is to preserve the topology of the shape. Bai *et al.* [23] introduce a convexity constraint for skeletonization and pruning that is used in contour partitioning with discrete curve evolution, and then use this skeletonization to match the skeleton graphs [24]. However, since their method for skeletonization and pruning removes unwanted branches iteratively, it might miss some part of the main skeleton, and hence, cannot preserve the topology of a shape completely. One of the most widely used algorithms is based on measuring the net outward flux by using Euclidean Distance Transform (EDT) of the binary image followed by a topology preserving thinning algorithm [19]. We use the method introduced by Dimitrov *et al.* [19] to calculate the net outward flux per unit area and detect the location of the pixels where conservation of energy principle is violated. EDT maps a binary image into a gray level image with value of each pixel represents its euclidean distance to the border of image. Given Euclidean distance of an image (D_E), we should first compute the gradient vector field (∇D_E), and then the divergence of this vector

field [19]. Mathematically, the divergence of the gradient vector field ($\nabla \cdot (\nabla D_E)$) is defined as the limit of the net outward flow of the field across the boundary of the area around the given point, while the area is shrinking to zero:

$$\nabla \cdot (\nabla D_E) = \lim_{S \to 0} \iint_C \frac{\nabla D_E \cdot \vec{n}}{S} dC \, , \qquad (1)$$

where C is the boundary, S is the area, and $\vec{n}$ is the normal vector of the boundary. Hence, we can calculate net outward flux at each point $P = (x, y)$ as follow:

$$Flux(P) = \sum_{i=1}^{8} \nabla D_E(Q_i) \cdot \vec{n} \, , \qquad (2)$$

where Q_i's are neighbor points to point P. According to the direction of the normal vector, we can determine that positive or negative flux values are representing drain or source of energy, where energy-draining points are internal skeletal points, and energy-generating points are external skeletal points. In the Figure 3b, the EDT of the binary image, in Figure 3a, is shown. Then, in Figure 3c the net outward flux for this Euclidean distance transform is computed.

By setting a threshold on flux values, initial binary skeleton map can be computed as depicted in Figure 3d. Because we are dealing with highly boundary-variant shapes, the skeleton map would contain a large number of unwanted branches that make the subsequent matching steps complicated. We need to develop an automated method to remove all such branches while keeping the main skeleton intact. We introduce a new method to prune the skeleton using fuzzy logic, which will be discussed in the next section. Our pruning algorithm needs to have the complete graph information of the skeleton including its vertices and edges' pixels coordinates. Therefore, the skeleton map is converted to a graph before the pruning step.

Converting a skeleton map to a graph consists of two steps, namely extracting vertices and then points of each edge. We will go through each step as follow:

- **Extracting Vertices**: For finding the vertices of the skeleton graph we need to scan the whole pixels of the image and based on the structure of other pixels around each pixel, we could decide weather it is a vertex or not. In this regard, we extract a 3×3 matrix around each pixel, which consists of its 8-connected neighbors. Then, in this matrix we build a local graph having pixels with value of "1" as its vertices. The connectivity of this graph is 4-connected neighbors, which means that 2 vertices are connected if and only if they are in one of the 4 main directions of each other (left, right, up, down). After that, in this graph we could calculate the Euler characteristic using its number of vertices and edges, as it is computed in algorithm 1. If the Euler characteristic of the graph is greater than 2, it shows that this point is on the crossing of three or more edges, hence, it is a vertex with a branch type. If it is 1, it means that this point is an end point vertex of an edge. When it equals 2, the point is a

simple edge point and not a vertex. Vertices extracted in this way for the skeleton in Figure 3d, is depicted (with a magnified part for a better representation) in Figure 3e. Red points in the image are branch points, and green ones are end points.

- **Extracting Edge Points**: After finding vertices in the graph, we should form the edge list of the graph. We start with a random end point and traverse its neighbors to reach to a branch point or other endpoints. If the neighbor pixel is not a branch point nor an endpoint, it would be added to the current edge's pixel list. When we reach a branch point, we should add another edge to the edge list, having that branch point as its first point, and start searching edge points for the next edge in the edge list. If we reach an end point, we just start searching edge points for the next edge in the edge list. This approach will be continued until there is no edge left unprocessed. Detailed algorithm of transforming skeleton map to graph is in Algorithm 1, and the result of finding edge list is shown in Figure 3f with different colors for different edges.

Algorithm 1 Skeleton2Graph

Input: Skeleton Map
Output: Branch Points, End Points, Edges List

1: **procedure** FIND VERTICES
2:     **for all** Points on Skeleton **do**
3:         *PointMatrix* ← find *8-Connected* Neighbors
4:         Filter *PointMatrix* by a *4-connected* Neighbors mask
5:         *EulerCharacteristic* ← #Vertices − #Edges
6:         **if** *EulerCharacteristic* > 2 **then**
7:             *BranchPoints* ← Point
8:         **else if** EulerCharacteristic = 1 **then**
9:             *EndPoints* ← Point
10:         **end if**
11:     **end for**
12: **end procedure**
13: **procedure** CREATE EDGE LIST
14:     *EdgeList{1}* ← Select one End Point randomly
15:     *EdgeNumber* ← 1
16:     **while** *EdgeNumber* ≤ # Edges in *EdgeList* **do**
17:         *SearchPoint* ← *EdgeList{EdgeNumber}*(end)
18:         *SearchMatrix* ← 8-Neighbors Connected to *SearchPoint*
19:         **for all** points in *SearchMatrix* **do**
20:             Set Value to −*EdgeNumber*
21:             **if** A point is in *BranchPoints* **then**
22:                 Add a new edge to *EdgeList* with having this Branch point as its first Point
23:                 *EdgeNumber* ← *EdgeNumber* + 1
24:             **else if** A Point in *EndPoints* **then**
25:                 *EdgeNumber* ← *EdgeNumber* + 1
26:             **else**
27:                 Add Points to *EdgeList{EdgeNumber}*
28:             **end if**
29:         **end for**
30:     **end while**
31: **end procedure**

2.4. Skeleton Pruning using Fuzzy Logic

Having high sensitivity to border variations, almost all algorithms for skeletonization need to be followed by a pruning stage in order to remove thin branches caused by boundary deformations. These branches may significantly change

(a) Binary image   (b) EDT   (c) Flux map

(d) Initial skeleton   (e) Graph vertices   (f) Graph edges
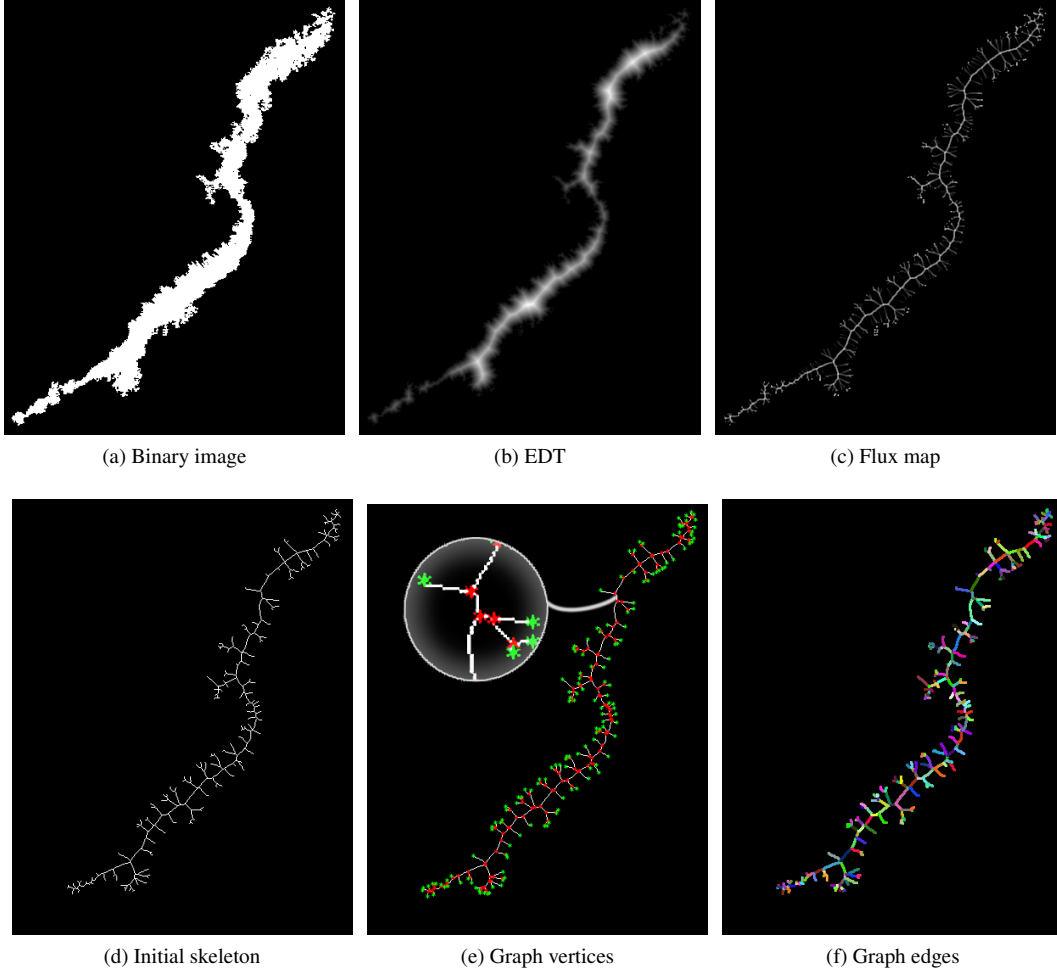
Figure 3: Different stages in the skeletonization process. (a) We start from extracting the binary image of the object. (b) We apply Euclidean Distance Transform on the binary image. (c) Using equation 2 calculate the flux map. (d) Apply a threshold to extract the initial skeleton. (e) & (f) Using Algorithm 1, extract vertices and edges of the initial skeleton.

the skeleton graph, and hence they should be treated carefully for the matter of topology preserving in skeletonization algorithms. This issue would be intensified in case of radar images and bow echo shapes, because they have drastic variations on their borders, as it is evident in radar images. There has been studies [23, 25, 26] investigating direct as well as indirect methods to address this issue. Most of these algorithms use Boolean logic in their decision to remove or keep the branches. The output of these algorithms is a crisp value attributed to each edge distinguishing branch edges from main skeleton edges. However, if we ask a person to do pruning on a skeleton graph, he or she would extract the main skeleton with an uncertainty to some extent. On the other hand, fuzzy logic introduces many-valued logic in close proximity to human decision making system [27, 28]. Hence, we propose an approach based on fuzzy inference system to prune skeleton graph and extract the main skeleton.

In our method, we use the outward flux values of the pixels as an input to the fuzzy inference system. Heuristically from raw images of flux values (Figure 3c), the higher the value of

the outward flux in each pixel, the more probable that the pixel is in the main skeleton. Therefore, based on this observation we can extract a feature for every edge connected to a vertex in the skeleton graph. In order to record vertices properties in the flux images, we form an array, called Γ, for each vertex with the length of the number of the edges linked to it. The value attributed to each edge e_j connected to the vertex V_i could be computed as follow:

$$\Gamma\{V_i, e_j\} = \frac{1}{M_j - 1} \sum_{P_j=2}^{M_j} (W_G(P_j) \cdot Flux(P_j)), \qquad (3)$$

in which, $j = 1, ..., N_i$ indicating the jth edge connected to V_i. N_i is the number of edges linked to V_i, M_j is the number of pixels in the jth edge, P_j is the index of pixels on the jth edge, starting from the vertex V_i, and $W_G(P_j)$ is the Gaussian weight for each pixel of edge e_j computed as follow:

$$W_G(P_j) = \exp\left(-\frac{\|P_j - V_i\|^2}{2\sigma^2}\right). \qquad (4)$$

5

Our proposed fuzzy inference system (FIS) consists of two components:

- FIS-1: Fuzzy inference system to compute degree of belief of each pixel to main skeleton edges.

- FIS-2: Fuzzy inference system to compute degree of belief of each pixel to branch edges.

The FIS-1 output, indicates that to what extent we believe an edge belongs to main skeleton. Afterwards, we use this value as an input to FIS-2 to compute the extent to which that we believe an edge belongs to branch edges. These values are the same for the pixels of the edge and varies among different edges. In following subsections we introduce these two fuzzy inference systems, their inputs, rules, and outputs. And then we go through the details of our algorithm for pruning skeleton.

2.4.1. Main Skeleton Fuzzy Inference System

We now describe the inputs, the outputs, and the operators used in the first fuzzy inference system (FIS-1). In this inference system, unlike the second one, because keeping the main skeleton correctly in the pruning step is more important than omitting branches, we need to have more resolution in the definition of the inputs and outputs. Accordingly, we use more number of membership functions with Gaussian type, that decay faster than linear, in this inference system, versus less number of membership functions with trapezoid type in the second one.

Fuzzy Inputs: FIS-1 has two inputs as follows:

Importance Value (I) : which indicates the importance of each vertex, and is generated from vertices properties of linked edges. The details of computing importance value would be described later. Based on variations in the importance values of different vertices, we can calculate the expected value and variance of this feature in an image. After statistically analyzing the expected value ($E\{I\}$) and variance (σ_I) of the importance value of all vertices, we come up with three Gaussian membership functions with their center on $[E\{I\} - 6\sigma_I, E\{I\}, E\{I\} + 6\sigma_I]$ and standard deviation (sigma) equal to σ_I. We call these membership functions *Low*, *Medium*, and *High*, according to their centers.

Edge Length (L_E) : One of the most important features for detecting main skeleton edges, is edge length. However, branches mostly happen where boundary is deformed with variations, and hence the skeleton would be furcated into too many small branches. As a result, we can use the edge length as an indicator for main skeleton pixels, alongside with other factors. Edge length in each image is random variable that we can find its expected value as $E\{L_E\}$, and its standard deviation as σ_{L_E}. Again with statistical analysis of edges, we attribute three different Gaussian membership functions with their centers on $[E\{L_E\} - 5\sigma_{L_E}, E\{L_E\}, E\{L_E\} + 5\sigma_{L_E}]$ and standard deviation (sigma) equal to σ_{L_E}. These membership functions are called *Small*, *Medium*, and *Long* respectively. Just in this case, we should make sure that the minimum value for edge length is not less than zero.

Fuzzy Output: This FIS has one output, that is, *Main Skeleton Degree of Belief* (Ψ_{MS}). This output represents the degree of belief on pixels to be on the main skeleton graph. The range of its value is between $[0, 1]$, and we define 5 different Gaussian membership functions as its fuzzy sets. The sigma value for these fuzzy membership functions is set to 0.05 and their centers are on $[0, 0.25, 0.5, 0.75, 1]$. These functions are named as follow: *Very Low*, *Low*, *Average*, *High*, and *Very High*. The output resulted from this FIS for the skeleton in Figure 3d is shown in Figure 8a. The higher the value in image, the higher degree of belief of main skeleton (Ψ_{MS}) on that edge. Fuzzy membership functions of the inputs and the output of this inference system for a sample skeleton is depicted in Figure 4.

Fuzzy Operators: In each fuzzy inference system we should define methods of integration of membership functions. First of all we should decide about the method of integrating different inputs in each rule, then the method for implication of the output in each rule, and at the end the method of aggregation of outputs from each rule. Hence, we choose these operators as follow:

- Fuzzy Operation: we choose the simplest method, that is, *min* for *AND* operations and *max* for *OR* operations.

- Implication Method: for the implication of the output we choose *min* operator.

- Aggregation: for the aggregation of the outputs, we use *max* operator.

2.4.2. Branch Fuzzy Inference System

The details of the second fuzzy inference system (FIS-2) are provided below.

Fuzzy Inputs: FIS-2 has three inputs including the output of FIS-1.

Main Skeleton Degree of Belief (Ψ_{MS}) : This is the output from the first FIS. However, for this FIS, as it was discussed before, we only consider two fuzzy membership functions, namely, *Low* and *High*. Instead of Gaussian, we choose trapezoid membership functions, because it would result in more fuzziness than before inherited from the definition of branches as well. The parameters of these two membership functions are $[0, 0, 0.3, 0.55]$ and $[0.4, 0.7, 1, 1]$, where the four parameters $[a, b, c, d]$ define a trapezoid membership function uniquely as follow:

$$mf(x, [a, b, c, d]) = max\left(min\left(\frac{x - a}{b - a}, 1, \frac{d - x}{d - c}\right), 0\right). \quad (5)$$

Edge Length (L_E): Because of the importance of edge length in distinguishing between main skeleton and branch edges, we use this feature in our second FIS, with the same range for its universe of discourse. But we merely define two membership functions in FIS-2 for this input, consisting of two trapezoid functions named *Small* and *Long*. The parameters of these two membership functions are
$[E\{L_E\} - 5\sigma_{L_E}, E\{L_E\} - 5\sigma_{L_E}, E\{L_E\} - 4\sigma_{L_E}, E\{L_E\} + \sigma_{L_E}]$ and
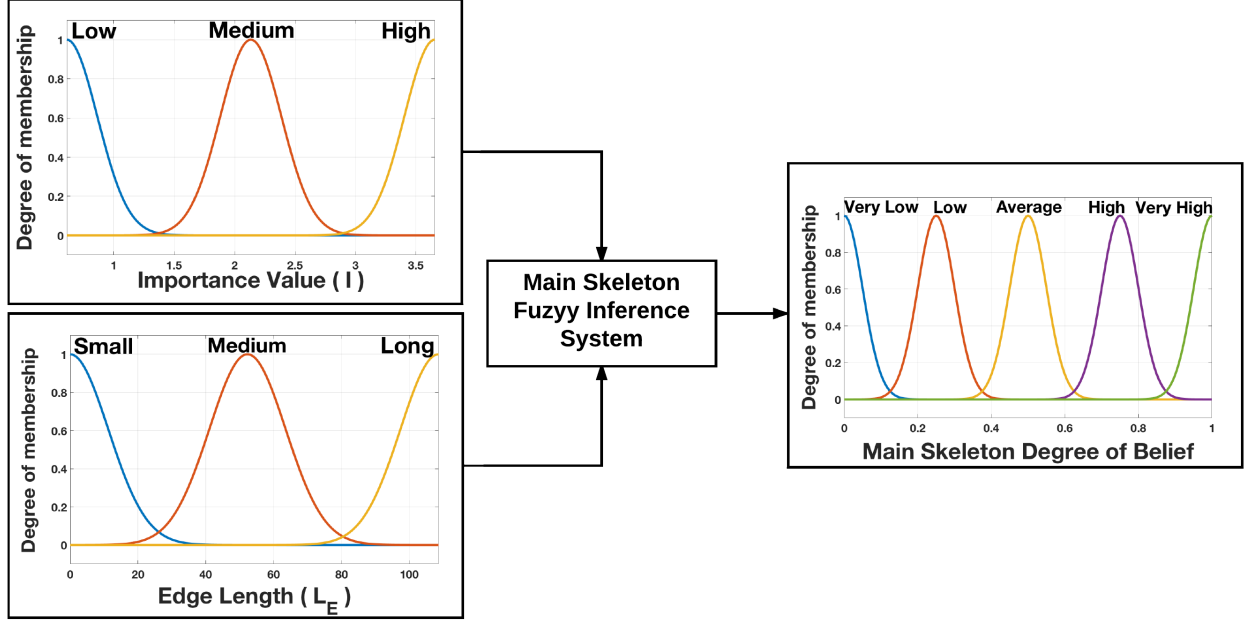
Figure 4: Inputs and the output membership functions of Main Skeleton fuzzy inference system for a sample skeleton

$[E\{L_E\} - \sigma_{L_E}, E\{L_E\} + 2\sigma_{L_E}, E\{L_E\} + 5\sigma_{L_E}, E\{L_E\} + 5\sigma_{L_E}]$, respectively. They are not symmetric because the distribution of edge length is more accumulated near zero.

Curvature Score (S_C) : In the course of searching for the main skeleton, we may encounter with a vertex that has two output edges, in which almost all of their properties are similar. The only difference between these two edges is their angle with the nearest main skeleton edge. The more this angle is close to zero, the more probable that we categorize the edge as a main skeleton edge rather than a branch edge. Therefore, we introduce Curvature Score for vertex V_i as follows:

$$S_C^{V_i}(\vec{e_{i_1}}, \vec{e_{i_2}}) = \cos(\theta_{i_1, i_2}) = \frac{< \vec{e_{i_1}}, \vec{e_{i_2}} >}{\|\vec{e_{i_1}}\| \, \|\vec{e_{i_2}}\|} \, , \qquad (6)$$

where $\vec{e_{i_1}}$ is the vector starting from the middle point of reference edge (or main skeleton edge) to V_i, and $\vec{e_{i_2}}$ is the vector starting from V_i to the middle point of the test edge. The universe of discourse for this input would lie in the range of $[-1, 1]$, and we choose two trapezoid membership functions on this range with the name of *Averted* and *Straight*. The parameters of these two membership functions are $[-1, -1, -0.7, 0.2]$ and $[-0.1, 0.7, 1, 1]$, respectively.

Fuzzy Output: The fuzzy output of this FIS is representing the degree of belief on edges to be member of branch edges, which is in the range of $[0, 1]$, and we call it Branch Degree of Belief (Ψ_B). We consider three membership functions for this output, namely, *Low*, *Average*, *High*, in which the first and the last one are trapezoid and the second one is a triangle membership functions with parameters $[0, 0, 0.2, 0.4]$, $[0.4, 0.5, 0.6]$, and $[0.6, 0.8, 1, 1]$, respectively. The result of this FIS on the skeleton of Figure 3d is depicted in Figure 8b. Higher values

in the image shows higher branch degree of belief (Ψ_B). Fuzzy membership functions of the inputs and the output of this inference system for a sample skeleton is depicted in Figure 5.

Fuzzy Operators: We use the same fuzzy operators as the first FIS for this FIS, that is, *min* for *AND* operation and *max* for *OR* operations in the rules, *min* operator for output implications, and *max* operator for aggregations.

2.4.3. Importance Value (I)

As it was mentioned in FIS-1, we have to compute value *I* for each vertex based on their flux values. Basically, this measure computes the importance level of each vertex or path based on its subsequent edges' flux values, plus its own flux value. To calculate the importance value of the vertices, we consider the skeleton graph as a directed tree starting from the best edge, with respect to the flux values of its pixels, as its root and all other edges connected to its vertices in their spatial order. Finding the best edge which has the highest flux value (the average of Γ values of its both vertices), we continue to move from both ends of the best edge toward other edges, until all the edges are covered. Because we are computing the importance value of each vertex in a predefined direction, it could be considered as two "Directed Tree"s (from both ends of the best edge) with vertices and edges in a hierarchical manner. Hence, in the course of computing importance value of a vertex we could include flux values of edges in the lower level linked to that vertex in the hierarchy. Sometimes flux values of edges on the main skeleton decrease (in proportion to their linked edges), which leads to a false detection by pruning algorithm, if we merely rely on flux values of each edge. Thus, this operation ensures to choose the main skeleton edges by increasing their importance values. As a result, we want to add depleted version of
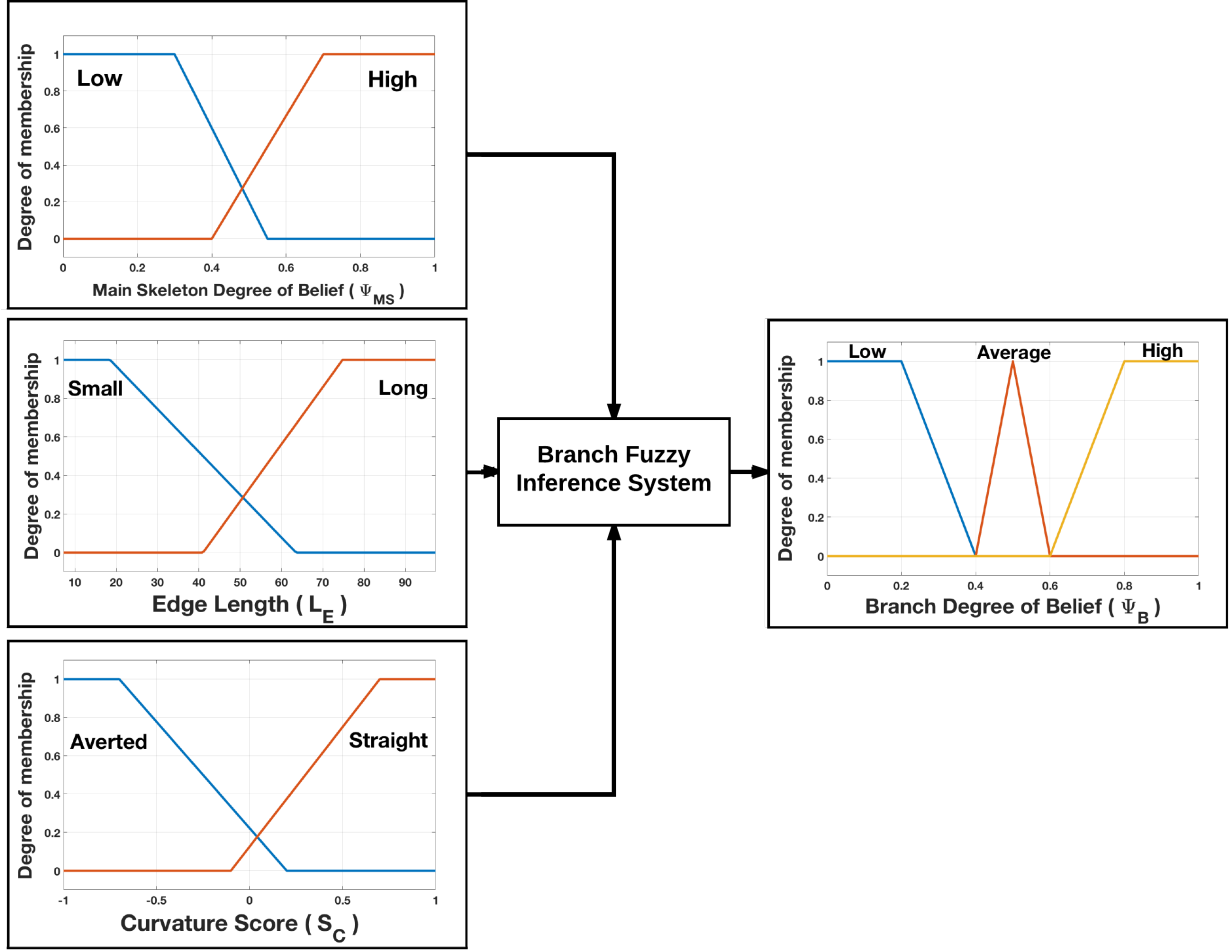
Figure 5: Inputs and the output membership functions of Branch fuzzy inference system for a sample skeleton

importance value of lower level vertices to importance value of current vertex. Hence, we can calculate the importance value for the vertex V_i in the recursive scheme as follows:

$$I(V_i, \Omega) = \begin{cases} C_d \times \sum_{k_i=1}^{M_{i,\Omega}} I(V_{k_i}, \Omega - 1), & \Omega > 0 \\ C_d \times \sum_{k_i=1}^{M_{i,\Omega}} \sum_{j_i=1}^{N_{i,\Omega}} \Gamma\{V_{k_i}, e_{j_i}\}, & \Omega = 0 \\ & \text{or } V_{k_i} \in EndPoints \end{cases} \tag{7}$$

in which, Ω shows the depth level needed to be included in the calculation of importance value for that Vertex. C_d is a damping factor between 0 and 1, $M_{i,\Omega}$ is the number of vertices linked to V_i in the level Ω, and $N_{i,\Omega}$ is the number of edges linked to V_i in the level Ω (note that this connection might be indirect). In summary, for calculating the importance value of a vertex we should consider vertices properties (Γ) of all subsequent vertices below this vertex in the tree. For further clarification, consider a simple skeleton graph in Figure 6, with 13 vertices and 11 edges. Assume that we found the best edge in the sense of flux value, and we want to calculate the importance value of vertex V_1 with $\Omega = 2$, hence, we should consider 2 layers of vertices lower than V_1 in the hierarchical graph depicted in Fig-

ure 6. These vertices are colored green on the figure, therefore based on equation 7, we could calculate this value:

$$I(V_1, \Omega = 2) = C_d \times (I(V_3, \Omega = 1) + I(V_4, \Omega = 1)) , \tag{8a}$$

$$I(V_3, \Omega = 1) = C_d \times \Gamma(V_3, e_{1-3}) , \tag{8b}$$

$$I(V_4, \Omega = 1) = C_d \times (I(V_6, \Omega = 0) + I(V_7, \Omega = 0)) , \tag{8c}$$

$$I(V_6, \Omega = 0) = C_d \times \Gamma(V_6, e_{4-6}) , \tag{8d}$$

$$I(V_7, \Omega = 0) = C_d \times \Gamma(V_7, e_{4-7}) , \tag{8e}$$

where you can see the recursive property of importance value. Thus, to find the importance value of vertex V_1, we should calculate the importance values of V_6 and V_7 from equations 8d and 8e, and substitute them in equation 8c. After calculating the importance value of V_3 and V_4 from equations 8b and 8c, we can substitute them in equation 8a and calculate the importance value of V_1. Note that as we go deeper in lower levels, the effect of their importance values is decreased because of C_d.

2.4.4. Pruning Algorithm

Using fuzzy inference systems with proper importance values of vertices and edges, the functionality of the pruning algorithm would be straight forward. We just need to define some
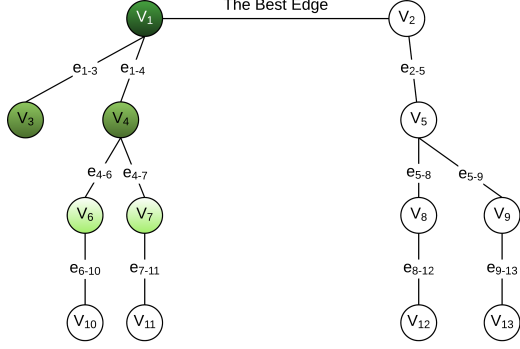
8

Figure 6: A simple skeleton graph with 13 vertices and 11 edges. Colored vertices are included in the calculation of the importance value of V_1 when $\Omega = 2$.

Figure 7: Belief Window (BW) versus Δ, and B_T. The slope of change in BW size would decrease by increasing Δ. This would be intensified by decreasing branch tolerance (B_T).

parameters to give users ability to decide to what extent they tolerate branches in an image and the maximum threshold of Ψ_B on an edge, to consider it as a branch. We define these parameters as follows:

$$B_T \equiv \text{Branch Tolerance} \in [0, 1] \,,$$
$$\Psi_B^\star \equiv \Psi_B \text{ Threshold} \in [0, 1] \,, \qquad (9)$$

where $B_T = 0$ means we do not tolerate any branches and we just want the medial axis. For example, if $B_T = 0$ and $\Psi_B^\star = 0.6$, then we would like to get rid of all edges that have Ψ_B greater than or equal with 0.6. Since by setting the Ψ_B threshold to 0.6, it means that we consider all edges on skeleton with Ψ_B greater than 0.6 as a branch. If B_T is set to 1, it does not mean that we want to keep all edges with Ψ_B less than $\Psi_B^\star$, but we want to constraint the decision based on the situation of each branch point. Take for instance, a branch point has two edges with both Ψ_B values less than $\Psi_B^\star$ and $B_T = 1$, but there is a large difference between their values, which makes us to choose the one with the lesser value. Hence, based on these two parameters and Ψ_B values in each branch point separately, we should form a Belief Window (BW) to filter desired values on that particular branch point. This window should always start from the minimum value among Ψ_B values of edges linked to a branch point, and can have a size in the form of equation below for the vertex V_i and set of edges linked to it in the lower level E_i:

$$BW(V_i, E_i) = B_T^{\Delta(V_i, E_i)} \times \Delta(V_i, E_i)^{f_1(B_T)} \times e^{f_2(\Delta(V_i, E_i))} \,, \qquad (10)$$

where

$$\Delta(V_i, E_i) \triangleq \Psi_B^\star - \min_{E_i} \Psi_B \,,$$
$$f_1(B_T) \triangleq \alpha + \beta B_T \,, \qquad (11)$$
$$f_2(\Delta(V_i, E_i)) \triangleq \kappa + \lambda \Delta(V_i, E_i) \,.$$

Hence, in this schema we always keep an edge with the lowest branch degree of belief (Ψ_B) in each branch point. Based on parameters defined by the user we form a belief window, which can decide whether we should keep other edges or not. This
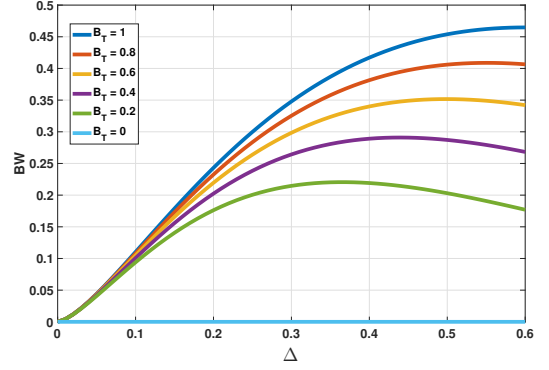
Algorithm 2 Pruning

Input: Skeleton Graph, Flux Values
Output: Pruned Skeleton Graph
1: $RootEdge \leftarrow$ Find the best edge with highest VP values.
2: $PointsQue \leftarrow$ Vertices($RootEdge$)
3: $QueNumber \leftarrow 1$
4: **while** $QueNumber \leq$ # Points in $PointsQue$ **do**
5:      $V_i \leftarrow PointsQue(QueNumber)$
6:      $E_i \leftarrow$ Edges linked to V_i in a lower level
7:      **for all** Edges in E_i **do**
8:          $\Psi_{MS_j} \leftarrow FIS_1(V_i, E_{i_j})$
9:          $\Psi_{B_j} \leftarrow FIS_2(V_i, E_i, \Psi_{MS_j})$
10:      **end for**
11:      $BW \leftarrow$ Form the BW based on equation 10.
12:      Choose candidate edges based on BW and their Ψ_{B_j} values
13:      Add end points of Candidate edges to $PointsQue$
14:      $QueNumber \leftarrow QueNumber + 1$
15: **end while**

function would satisfy aforementioned property of belief window for choosing branches. Parameters of lines in f_1 and f_2 can be set heuristically. For example, we can set them as follow: $\alpha = 1.5$, $\beta = 0.2$, $\kappa = 1.5$, and $\lambda = -2.5$. Changes in the size of belief window with changing Δ and B_T is depicted in Figure 7. This window size generally would increase when the Δ increases. The slope of this change is high when Δ is small, however, as the gap between $\Psi_B^\star$ and minimum branch degree of belief in a branch point goes high, it decreases. When this window is formed, in each branch point we can decide which edges to keep or omit. Detailed pruning algorithm using fuzzy logic is in Algorithm 2, which takes a skeleton graph and its associated flux map, and calculate the pruned skeleton graph. It starts from one edge and try to find edges that should be kept based on the criteria discussed before. The pruned skeleton of Figure 3d with zero branch tolerance is in the Figure 8c.

2.5. Skeleton Context

Shape Context [29] as a powerful shape descriptor represents a rough distribution of all other points with respect to a selected point in terms of distance and angle. It has quite number of applications in object recognition [30], pose recognition [31], animation construction [32], to name but a few. Shape context is used to find correspondences between samples from border
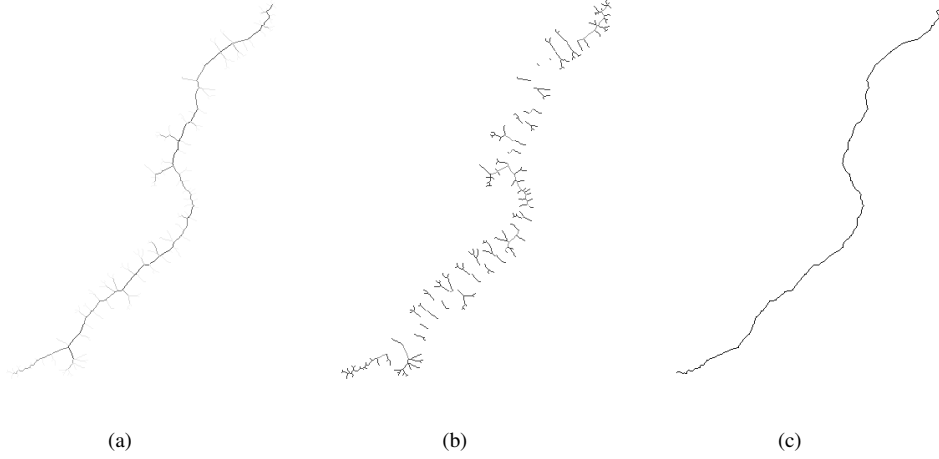
9

Figure 8: Output of pruning algorithm: (a) main skeleton degree of belief, (b) branch degree of belief, (c) Pruned skeleton. In (a) and (b) images are in grayscale, and higher values represent higher degree of beliefs

of two shapes, and then find the cost of matching two shapes using bipartite graph matching. After that, parameters for an affine transform are extracted using thin plate spline (TPS), in order to map points from one shape to their correspondences in the other shape with warping the coordinates. Finally, a notion of shape distance for recognition purposes is exploited.

As there are a lot of fluctuations over the boundaries of the shapes in radar images, these make object matching with boundary samples less effective, and it may result in false matching. On the other hand, matching objects using skeleton samples sounds more robust in the sense that pruned skeleton contains complete shape topology regardless of its boundary variations. Hence, we use *shape context* to introduce a new descriptor called skeleton context. As it is shown in an example in Figure 9, skeleton context is log-polar histogram, formed for each sample point on the skeleton. For each sample point P_i, the center of this log-polar histogram is located on that sample point, then each bin in the histogram represents the number of sample points in the specific angle and range of distance from the center (i.e. P_i) determined by that bin. We use the notation of $H_{SC}(P_i, r_{k_1}, \theta_{k_2})$, to show the value of skeleton context's histogram for point P_i, in the (r_{k_1}, θ_{k_2}) bin. For instance, when $H_{SC}(P_i, r_m, \theta_n) = 10$, it means that in the distance range of $r_{m-1} \le r < r_m$ and in the angle range of $\theta_{n-1} \le \theta < \theta_n$ from the point P_i in the skeleton, there are 10 other sample points. Basically, these histograms for each point visualize the distribution of other points on the skeleton with respect to that point, and hence it could play the object descriptor role for the shape matching purposes. As a result, we could use these descriptors as the feature data for bow echo detection in the next step. The skeleton context can be calculated using the following equation:

$$
\begin{aligned}
H_{SC}(P_i, r_{k_1}, \theta_{k_2}) =& |Bin(P_i, r_{k_1}, \theta_{k_2})| , \\
Bin(P_i, r_{k_1}, \theta_{k_2}) =& \{ X \in \mathbb{S} \mid r_{k_1-1} \le \|X - P_i\|_2 < r_{k_1} \bigcap \theta_{k_2-1} \\
& \le \angle(X, P_i) < \theta_{k_2} \} ,
\end{aligned}
$$

(12)

where $|.|$ shows the number of members in a set, P_i is a sample point on the skeleton that we want to calculate its skeleton context, $\mathbb{S}$ is the set of sample points in the skeleton, and $\angle(X, P_i)$ calculate the angle of a vector from P_i to X when P_i is on the origin of coordinates, with respect to the horizontal coordinate. In Figure 9 the skeleton context is computed for two points of two objects, which matched together in our algorithm.

3. Bow Echo Classification and Detection

With skeleton context defined in previous section, we are able to extract features from objects in radar images and use them in the recognition process. In the following subsections, we introduce our proposed model for learning features of bow echoes and implementing a classifier in order to detect bow echoes in tons of objects extracted from radar images. First, we introduce four indicators that can help us to define distance metric between two skeletons. Then, we impose neighboring cost to enforce partial shape matching. In the end, we use the defined distance metric, to find the prototypes of the bow echo class, and then we use these prototypes in the classification step.

3.1. Shape Matching with Skeleton Context

In this section we want to introduce four indicators to measure the quality of the matched skeletons. The procedure for Skeleton matching is nearly the same with the method introduced in [29], that is, instead of shape context, we use our proposed descriptor skeleton context. Defined in [29], we can compute the cost of mapping each skeleton point P_i^1 in image 1, to each skeleton point P_j^2 in image 2, which simply is the normalized difference between skeleton contexts of each pair of points in two images:

$$
C(P_i^1, P_j^2) = \frac{1}{2} \sum_{k_1, k_2} \frac{\left(H_{SC}(P_i^1, r_{k_1}, \theta_{k_2}) - H_{SC}(P_j^2, r_{k_1}, \theta_{k_2}) \right)^2}{H_{SC}(P_i^1, r_{k_1}, \theta_{k_2}) + H_{SC}(P_j^2, r_{k_1}, \theta_{k_2})} .
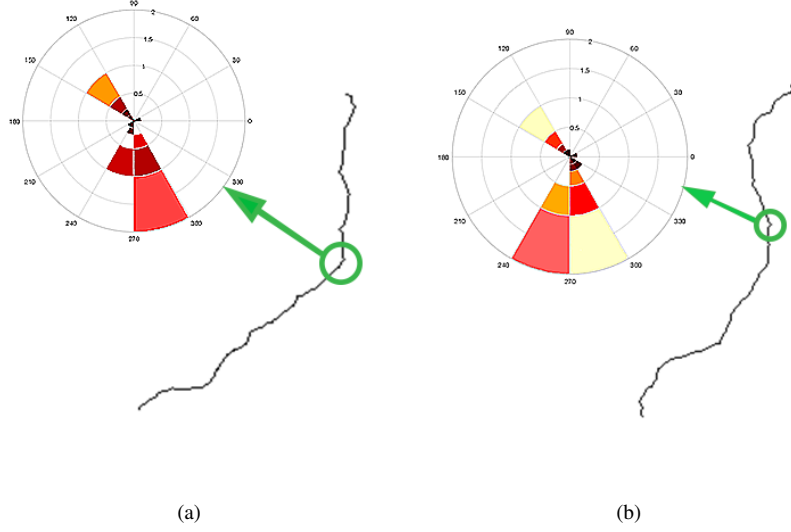$$

(13)

(a)   (b)

Figure 9: Skeleton Context of 2 points on different skeletons that are matched based on the algorithm.

Having the cost of all possible mapping, we can use one of the algorithms designed to solve the bipartite graph matching, such as Hungarian method [33], which finds the minimum cost solution for matching points in image 1 to image 2. We define a threshold for the cost of matching, which indicates that if the minimum cost of matching one point from image 1 to the points of image 2 is greater than that threshold, then we announce that there is no matching point for this sample point in image 1. This would end in having some points without a proper pair from other image, and hence the matching ratio would be less than 1. This is necessary for having partial shape matching, which would be described in the next section. Next, we use an affine transformation to warp coordinates of one image, in order to map its skeleton to other image skeleton. As mentioned, for this step we could use TPS interpolation which tries to minimize the bending energy as it is defined in [29]. In warping coordinates, we need an indicator that shows the intensity of changes on shapes in the transformation . For instance, if the transformation is just a simple rotation or relocation, this indicator should be low, which means the transformation has not warped coordinates extensively. But it would be high, if the transformation is warping coordinates significantly to map the points together. If the affine transformation could be written in mathematical form as:

$$\vec{y} = f(\vec{x}) = A\vec{x} + \vec{b} , \tag{14}$$

with matrix A as linear map and vector $\vec{b}$ as the offset for translation, then we can write our indicator for affine transformation as follows:

$$C_A = \log \frac{\sigma_1(A)}{\sigma_2(A)} , \tag{15}$$

where $\sigma_i(A)$ shows i-th singular value of matrix A, with $\sigma_1 \geq \sigma_2$. The more C_A is closer to zero, the more the skeleton of two shapes are similar, and the less coordinates are warped. Overall,

we can use four different indicators for defining the distance between two skeletons:

- *Matching Cost* (C_{MC}) : This is defined based on the cost of matching points in two shapes, as it was computed in equation 13.

- *Bending Energy* (C_{BE}) : The energy that TPS wants to minimize, which is described in [29].

- *Affine Indicator* (C_A) : which is defined in equation 15.

- *Matching Ratio* (C_{MR}) : It represents the ratio of the number of sample points in image 1, that we could match with points in image 2; to the total number of sample points. As it was discussed, some points would not match to any points if the cost of matching to the points in the other shape is greater than a predefined cost. This would allow the algorithm to achieve partial matching.

3.2. Neighboring Effect

As it was mentioned, we need partial shape matching, as bow echoes have a tail in addition to the bow part in some cases, and this tail might be different among various bow echoes. Therefore, we should add an alteration to the shape matching part, in order to include partial shape matching in our algorithm. To do so, after the first iteration of shape matching, we can learn the initial mapping between sample points of two images. Because in our algorithm for extracting the edge list, points are listed in accordance with their spatial order, we can use this ordinal positions of sample points to define neighbors. For instance, if $(m - 1)$-th and $(m + 1)$-th sample points in image 1 are mapped respectively to $(n - 1)$-th and $(n + 1)$-th sample points in image 2 , then we expect m-th sample point in image 1 to be mapped as close as possible to n-th sample point in image 2. This is what we call neighboring effect, and we want to impose this

11

constraint in the shape matching algorithm by adding a Neighbor Cost to the cost introduced in equation 13. This Neighbor Cost for the point m in the image 1 could be in the form of:

$$C_N(n, m) = \epsilon_N \left[1 - \exp\left(-\frac{((n - m) - E\{\delta_N\})^2}{2\sigma^2}\right) \right], \qquad (16)$$

where ϵ_N is the maximum amplitude of this cost, and random variable δ_N is the difference between sample points' numbers in image 1 with respect to the their mapped sample points' in image 2. This cost would be a function of indexes of sample points in image 2 (*i.e.* n) and image 1 (*i.e.* m), hence for each pair of (m, n) we would calculate a neighboring cost according to this function to be added to their mapping cost. For instance, if the average of the mapping differences$(E\{\delta_N\})$ is 5, we expect to map the point 10 in image 2, to the point 5 in image 1. Based on equation 16, it would add 0 to the cost of mapping pair of $(10, 5)$, however it increases as m deviating from 5. This Gaussian shape function would try to keep mapping of each sample point in accordance to its neighbors.

3.3. Distance Definition and Prototype Extraction

Because there is no simple metric to distinguish between the shape of two different skeletons, defining the distance between them becomes more challenging. However, after introducing indicators for matching two skeletons in section 3.1, we should be able to define a distance metric based on the combination of those indicators, and learn a classifier using that distance metric. In order to make this process more straightforward, we employ an iterative framework to define the distance metric and extract some prototypes of a bow echo class for the classification purposes, simultaneously.

Combining the skeleton matching indicators to define the distance metric, we use Principle Component Analysis (PCA), and use this distance metric to find the best prototypes representing the bow echo class. Having abundant types of bow echoes in radar images, we can use *K-medoids* algorithm [34] to find prototypes in the bow echo class. Thereafter, these prototypes are used as the representatives of the bow echo class.

K-medoids algorithm after initialization and finding k initial medoids iterate between these two steps:

- **Assignment**: In this step we should partition the feature space based on the distance of the points to the medoids. Each point should be assigned to medoid $\underline{m}_i$ if and only if the distance of that point has the following property:

$$D(\underline{x}, \underline{m}_i) \leq D(\underline{x}, \underline{m}_j), \qquad \forall j \neq i, \qquad (17)$$

where $D(., .)$ is the distance between two points, $\underline{x}$ is feature points in feature space, and $\underline{m}_j$s are medoids.

- **Update**: After assigning each point to a medoid, we can form clusters. Now we should find the point that has the minimum distance to all other points in a cluster. This point would be a new medoid.

As one can infer, to perform k-medoids algorithm, we need to have a well-defined distance metric between two points in the feature space (*i.e.*, two skeletons in the real world). In Section 3.1, in addition to the three matching costs showing the difficulty of that matching task, we define a matching ratio that shows how successful the task is. This parameter ranges from 0.5 to 1, where the greater the ratio the more successful the task. Hence, we reflect the extent of successfulness of the task on those three costs by inversely mapping the matching ratio from [0.5, 1] to [0, 1] and multiplying it to those costs. We use the exponential encoding function of $e^{(05 - r)/0.1}$ to approximately do the inverse mapping, which maps $r = 0.5$ to 1 and $r = 1$ to 0.0067.

After constructing the revised costs by reflecting the matching ratio on those three costs, now we can define our distance in this three dimensional feature space, by applying PCA, in order to reduce the dimension from three to one. Note that, applying PCA would reduce a high-dimensional feature space to a low-dimensional feature space with highest variation, and hence it would be helpful for classification and discrimination purposes. If we perform matching on all skeleton pairs available in the dataset, we would have $r = N^2/2$ rows of matching costs in feature space (N is the total number of skeletons in the dataset). Therefore, the feature space would be a matrix $C_{r \times 3}$, which has r samples and 3 dimensions. Each row in the feature matrix shows the matching costs of two skeletons in the dataset. What PCA is doing is simply as follow:

$$\underline{t}_{r \times 1} = C_{r \times 3} \times \underline{\omega}_{3 \times 1}, \qquad (18)$$

where $\underline{\omega}$ is the eigenvector associated with the highest eigenvalue of the matrix $C^T C$, and $\underline{t}$ is the reduced-dimension feature vector. Thus, the coefficients of $\underline{\omega}$ can be used to define the distance metric as follow:

$$d(i, j) = \underline{\omega}(1) \cdot c'_{ij} + \underline{\omega}(2) \cdot e'_{ij} + \underline{\omega}(1) \cdot a'_{ij}, \qquad (19)$$

where c'_{ij}, e'_{ij}, and a'_{ij} are revised matching cost, bending energy, and affine indicator to match skeleton i to skeleton j respectively. Their definition is stated in the algorithm 3.

As we define the distance metric and the way to extract prototypes, we can make them happen at the same time in an iterative fashion. To do so, we design an algorithm, which iterates on the coefficients of the distance metric to extract prototypes and update the distance metric according to new prototypes, until it converges.

In a shape matching scenario, distance of a shape to a class would be its minimum distance to one of the class's prototypes. Hence, if we have the prototypes for the bow echo class, we could reduce the number of rows in the feature matrix by just keeping the matching costs of each skeleton to its nearest prototype. This would reduce r to N, which means we have one row for each skeleton in the dataset. However, this would be tricky, since by finding some new prototypes in a class, the feature matrix would change in accordance with the new prototypes. Hence, to rectify this issue and finding the optimum distance metric based on the prototypes, we design algorithm 3. In each step, we first find the prototypes according to the distance metric defined in the last step from equation 19, and then with re-

Algorithm 3 Prototypes and Distance

Input: Matching Cost ($C_{MC} = \begin{bmatrix} c_{ij} \end{bmatrix}$), Bending Energy ($C_{BE} = \begin{bmatrix} e_{ij} \end{bmatrix}$), Affine
Indicator ($C_A = \begin{bmatrix} a_{ij} \end{bmatrix}$), and Matching Ratio ($C_{MR} = \begin{bmatrix} r_{ij} \end{bmatrix}$)
Output: Prototypes, Distance Coefficients

1: *Initialization:*

- $C'_{MC} = \begin{bmatrix} c'_{ij} \end{bmatrix} = \begin{bmatrix} c_{ij} \cdot e^{(05 - r_{ij})/0.1} \end{bmatrix}$

- $C'_{BE} = \begin{bmatrix} e'_{ij} \end{bmatrix} = \begin{bmatrix} e_{ij} \cdot e^{(05 - r_{ij})/0.1} \end{bmatrix}$

- $C'_A = \begin{bmatrix} a'_{ij} \end{bmatrix} = \begin{bmatrix} a_{ij} \cdot e^{(05 - r_{ij})/0.1} \end{bmatrix}$

- $\underline{\omega}_0 \leftarrow [0, 0, 0]$ and $\underline{\omega}_1 \leftarrow [1, 1, 1]$

- *Distance Matrix* (D) $\leftarrow \underline{\omega}_1(1) \cdot C'_{MC} + \underline{\omega}_1(2) \cdot C'_{BE} + \underline{\omega}_1(3) \cdot C'_A$

- $n \leftarrow 1$

2: **while** $\|\underline{\omega}_n - \underline{\omega}_{n-1}\|^2 \geq \epsilon$ **do**
3:      Prototypes ($m_j, j = 1, ..., k$) $\leftarrow$ Randomly assign prototypes
4:      **while** Prototypes change **do**
5:          **Assignment**: For each point find the cluster index as follow:
6: $$j^* = \underset{j}{\operatorname{argmin}}\left(D(\underline{x}_i, \underline{m}_j)\right)$$
7:          **Update**: Find new prototype in each cluster:
8: $$m'_j = \underset{i_j}{\min}\left(\Sigma_{l_j=1}^{L_j} D(\underline{x}_{i_j}, \underline{x}_{l_j})\right)$$
9:      **end while**
10:      *Feature Set* ($C_{N \times 3}$) $\leftarrow$ update feature set to have the matching costs of
         each skeleton to its nearest prototype
11:      $n \leftarrow n + 1$
12:      $\underline{\omega}_n \leftarrow$ Coefficient of PCA on *Feature Set*
13: **end while**

---

spect to the new prototypes update the feature matrix. Next, update the distance metric coefficients by applying PCA to the new feature matrix. It iterates until it converges to consistent coefficients. In the first step, all costs would contribute equally to the definition of the distance metric. The detailed algorithm is in 3. The output of this algorithm would be k prototypes representing bow echo class, and the distance coefficients to map three-dimensional feature space into one dimension. For instance, when we use $k = 8$ on our dataset for year 2008, the resulting prototypes for the bow echo class are shown in Figure 10.

3.4. Classifier

After defining prototypes for the bow echo class and distance coefficients, in order to decide whether a skeleton image belongs to bow echo class or non-bow echo class, we just need to find the minimum distance between skeleton image and bow echo prototypes. The distance of two skeletons is defined as a linear combination introduced in equation 19. As a classifier we use Mixture Discriminant Analysis (MDA) [35], which is generalized version of Linear Discriminant Analysis (LDA). In MDA, we consider each class has R_m prototypes with Gaussian distributions, and next, using Expectation Maximization (EM) algorithm [36] to find the Gaussian-distributed parameters and probability of each sample in each Gaussian-distributed subclass. Note that, these prototypes in EM algorithm are different from what we extracted in Section 3.1. The feature that we are training the classifier on, is the distance of each skeleton from its nearest prototype defined in Algorithm 3. The EM algorithm alternates between these two steps [35]:

- *Expectation Step* (E-step): Given the parameters for the distributions of R_m sub-classes in class m, we should assign a weight for each sample in each sub-class, with total sum of probabilities equal to one.

- *Maximization Step* (M-step): Using weights computed in the E-step, in order to compute weighted Maximum Likelihood estimation for parameters of each sub-class distribution.

After training and finding the parameters for sub-class distributions in both bow echo and non-bow echo classes, our classifier assess the weight of new coming samples for each subclass in two classes. This would determine the class of that sample based on the label of the nearest subclass to the sample.

4. Case Study

Using skeletonization approach and shape matching algorithm with skeleton context introduced in sections 2 and 3 respectively, alongside with the classifier defined above, we are able to detect bow echoes in radar images automatically with high rate of accuracy. To test this approach and the classifier, we use our radar database for a case study.

4.1. Training Data

Our database consists of US radar images taken by NEXRAD radars in the whole year of 2008. We have chosen that year because it had a large number of severe weather activities. The techniques developed, however, are general and applicable to any year. We search the whole year images to find those dates that bow echo happened in United States, and succeed to label 89 distinct days with bow echo during 2008 including $1,148$ radar images. After that, we extract skeleton of regions of interest in each radar images and label them as bow echo and non-bow echo classes. In each image that we can spot a bow echo, there would be some other parts that are not bow echo but would be captured as regions of interest, for their reflective signal amplitudes are similar to bow echo. From these images, we label $1,148$ bow echo samples and 443 non-bow echo samples.

4.2. Prototype Extraction

As it was explained in section 3.4, we need to implement k-medoids algorithm [37] to find k different bow echoes as prototypes of bow echo class. Consequently, we first find the matching costs between all bow echoes by running shape matching algorithm pairwise on all bow echo class samples. After finding matching costs matrix between all pairs of bow echoes, by running k-medoids algorithm, k bow echo prototypes are extracted, as it is depicted in Figure 10, for $k = 8$.

4.3. Classification

The last step would be the training of the MDA classifier and classification process. For this step, we use cross-out validation to get more accurate results on our database. 20-fold cross-out validation would chunk data to 20 parts, each of which containing both bow echo and non-bow echo samples. In each
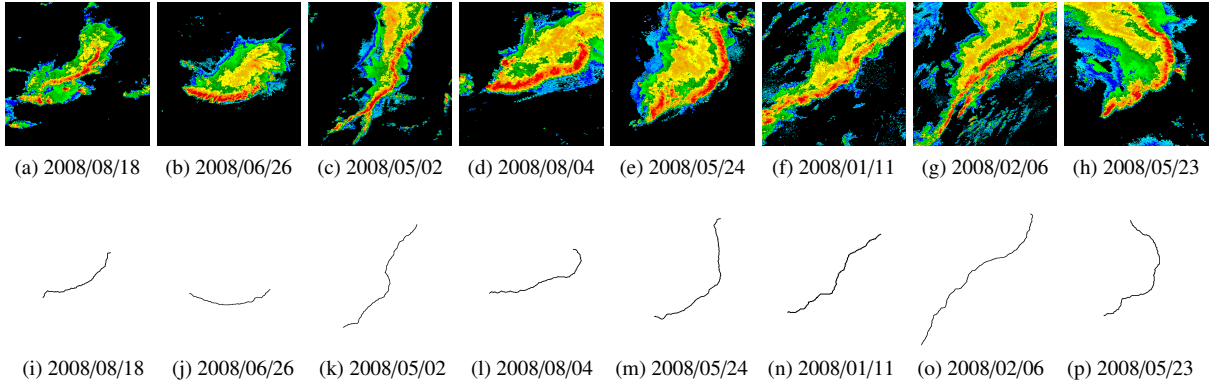
(a) 2008/08/18   (b) 2008/06/26   (c) 2008/05/02   (d) 2008/08/04   (e) 2008/05/24   (f) 2008/01/11   (g) 2008/02/06   (h) 2008/05/23

(i) 2008/08/18   (j) 2008/06/26   (k) 2008/05/02   (l) 2008/08/04   (m) 2008/05/24   (n) 2008/01/11   (o) 2008/02/06   (p) 2008/05/23

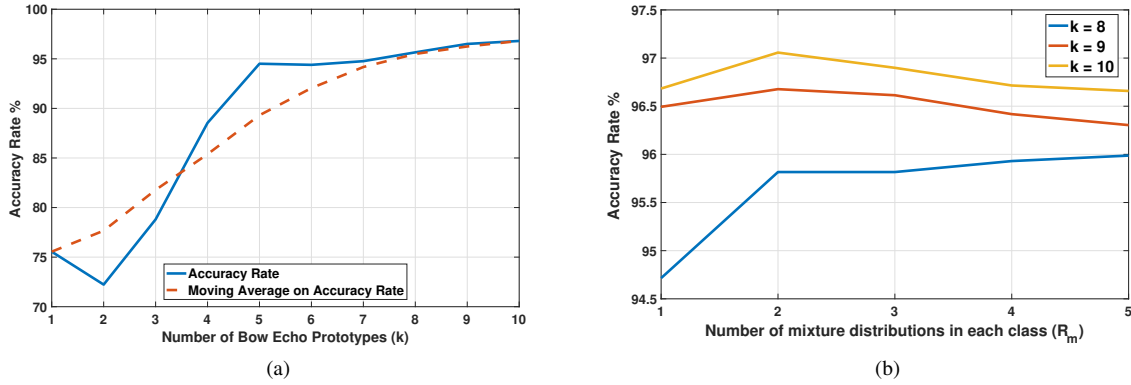Figure 10: Bow echo prototypes with $k = 8$. each figure shows a bow echo prototype with its extracted skeleton

(a)

(b)

Figure 11: Accuracy Rate versus (a) number of bow echo prototypes, and (b) number of mixture distributions in each class.

iteration, one chunk of data would be considered as *test* data, and the other 19 chunks of data would be used as *training* data. The results of using MDA algorithm with 8, 9, and 10 prototypes ($k = 9, 8, 10$) is shown in Figure 11b, which reveals that the best option for number of distributions is $R_m = 2$. The effect of the number of bow echo prototypes is computed in Figure 11a. Results, indicate that overall it has increasing order with adding more prototypes, but it became approximately constant after 5 prototypes. Because for finding bow echo prototypes, the k-medoids algorithm should run separately each time, these prototypes could be completely different. For instance, for $k = 3$ and $k = 4$, the k-medoids algorithm can choose totally distinct prototypes. Thus, as our proposed algorithm depends on topological features of these distinct prototypes, the results of classification can vary based on these features. To compensate this effect, we apply moving average on the results, which makes it more reliable and robust against randomness inherent in choosing prototypes. We can go beyond ten prototypes to get better results, but the disadvantages of increasing computational time by adding more prototypes is higher than the benefits of small portion of improvement in accuracy rate.

5. Conclusions and Future Work

In this paper, we presented a novel computational approach for detecting bow echo patterns in radar images. Meteorologists can use our method to record bow echoes automatically and with high accuracy. In addition to detection, the next step in this research would be forecasting of bow echoes and severe weather conditions associated with them. This could be possible in this framework as well. With the help of affine indicator introduced in section 3.1, we can track changes in a line over some periods of time to see whether it is going to deform to a bow echo shape or not. Hence, this framework could be exploited for further developing of forecasting techniques.

Beyond the meteorological point of view, this research suggests more opportunities for future research direction. Shape matching is one of the most challenging areas in computer vision from early stages of formation of the field. This research suggests a new and robust descriptors for shapes to be used in shape matching context. On the other side, the innovative approach for skeletonization and skeleton pruning using fuzzy logic can be used in other schemes in image processing and computer vision for extracting well-structured skeletons in close proximity to human vision.

Acknowledgments

References

[1] B. A. Klimowski, M. R. Hjelmfelt, M. J. Bunkers, Radar observations of the early evolution of bow echoes, Weather and Forecasting 19 (4) (2004) 727–734.

[2] B. A. Klimowski, M. J. Bunkers, M. R. Hjelmfelt, J. N. Covert, Severe convective windstorms over the northern high plains of the united states, Weather and Forecasting 18 (3) (2003) 502–519.

[3] C. Davis, N. Atkins, D. Bartels, L. Bosart, et al., The bow echo and mcv experiment, Bulletin of the American Meteorological Society 85 (8) (2004) 1075.

[4] R. W. Przybylinski, The bow echo: Observations, numerical simulations, and severe weather detection methods, Weather and Forecasting 10 (2) (1995) 203–218.

[5] L. Zhou, C. Kambhamettu, D. B. Goldgof, K. Palaniappan, A. Hasler, Tracking nonrigid motion and structure from 2d satellite cloud images without correspondences, IEEE transactions on Pattern Analysis and Machine Intelligence 23 (11) (2001) 1330–1336.

[6] Y. Zhang, S. Wistar, J. Li, M. A. Steinberg, J. Z. Wang, Severe thunderstorm detection by visual learning using satellite images, IEEE Transactions on Geoscience and Remote Sensing 55 (2) (2017) 1039–1052.

[7] Y. Zhang, S. Wistar, J. A. Piedra-Fernández, J. Li, M. A. Steinberg, J. Z. Wang, Locating visual storm signatures from satellite images, in: IEEE International Conference on Big Data, 2014, pp. 711–720.

[8] B. K. Horn, B. G. Schunck, Determining optical flow, Artificial Intelligence 17 (1-3) (1981) 185–203.

[9] S. G. Narasimhan, S. K. Nayar, Contrast restoration of weather degraded images, IEEE Transactions on Pattern Analysis and Machine Intelligence 25 (6) (2003) 713–724.

[10] P. S. Quinan, M. Meyer, Visually comparing weather features in forecasts, IEEE transactions on visualization and Computer Graphics 22 (1) (2016) 389–398.

[11] M. M. Kamani, F. Farhat, S. Wistar, J. Z. Wang, Shape matching using skeleton context for automated bow echo detection, in: Big Data (Big Data), 2016 IEEE International Conference on, IEEE, 2016, pp. 901–908.

[12] T. T. Fujita, Manual of Downburst Identification for Project NIMROD, Satellite and Mesometeorology Research Project, Department of the Geophysical Sciences, University of Chicago, 1978.

[13] Iowa Environmental Mesonet, Documentation on IEM generated nexrad composites (2001).
URL http://mesonet.agron.iastate.edu/docs/nexrad_composites/

[14] H. Sundar, D. Silver, N. Gagvani, S. Dickinson, Skeleton based shape matching and retrieval, in: Shape Modeling International, 2003, pp. 130–139.

[15] C. Hong, J. Yu, J. Wan, D. Tao, M. Wang, Multimodal deep autoencoder for human pose recovery, IEEE Transactions on Image Processing 24 (12) (2015) 5659–5670.

[16] R. Ogniewicz, M. Ilg, Voronoi skeletons: Theory and applications, in: IEEE Computer Society Conference on Computer Vision and Pattern Recognition, 1992, pp. 63–69.

[17] K. Siddiqi, A. Shokoufandeh, S. J. Dickinson, S. W. Zucker, Shock graphs and shape matching, International Journal of Computer Vision 35 (1999) 13–32.

[18] B. Kégl, A. Krzyzak, Piecewise linear skeletonization using principal curves, IEEE Transactions on Pattern Analysis and Machine Intelligence 24 (1) (2002) 59–74.

[19] P. Dimitrov, C. Phillips, K. Siddiqi, Robust and efficient skeletal graphs, in: IEEE Conference on Computer Vision and Pattern Recognition, Vol. 1, 2000, pp. 417–423.

[20] F. Reinders, M. E. Jacobson, F. H. Post, Skeleton graph generation for feature shape description, in: Data Visualization, Springer, 2000, pp. 73–82.

[21] P. K. Saha, G. Borgefors, G. S. di Baja, A survey on skeletonization algorithms and their applications, Pattern Recognition Letters 76 (2016) 3–12.

[22] H. Blum, Biological shape and visual science (part i), Journal of Theoretical Biology 38 (2) (1973) 208–287.

[23] X. Bai, L. J. Latecki, W.-Y. Liu, Skeleton pruning by contour partitioning with discrete curve evolution, IEEE Transactions on Pattern Analysis and Machine Intelligence 29 (3) (2007) 449–462.

[24] X. Bai, L. J. Latecki, Path similarity skeleton graph matching, IEEE Transactions on Pattern Analysis and Machine Intelligence 30 (7) (2008) 1282–1292.

[25] H. Liu, Z.-H. Wu, X. Zhang, D. F. Hsu, A skeleton pruning algorithm based on information fusion, Pattern Recognition Letters 34 (10) (2013) 1138–1145.

[26] W. Shen, X. Bai, X. Yang, L. J. Latecki, Skeleton pruning as trade-off between skeleton simplicity and reconstruction error, Science China Information Sciences 56 (4) (2013) 1–14.

[27] L. A. Zadeh, Fuzzy sets, Information and Control 8 (3) (1965) 338–353.

[28] J. Kacprzyk, Studies in Fuzziness and Soft Computing, Springer, 2000.

[29] S. Belongie, J. Malik, J. Puzicha, Shape matching and object recognition using shape contexts, IEEE Transactions on Pattern Analysis and Machine Intelligence 24 (4) (2002) 509–522.

[30] Z. Ren, J. Yuan, J. Meng, Z. Zhang, Robust part-based hand gesture recognition using kinect sensor, IEEE Transactions on Multimedia 15 (5) (2013) 1110–1120.

[31] J. Shotton, T. Sharp, A. Kipman, A. Fitzgibbon, M. Finocchio, A. Blake, M. Cook, R. Moore, Real-time human pose recognition in parts from single depth images, Communications of ACM 56 (1) (2013) 116–124.

[32] J. Yu, D. Liu, D. Tao, H. S. Seah, Complex object correspondence construction in two-dimensional animation, IEEE Transactions on Image Processing 20 (11) (2011) 3257–3269.

[33] C. H. Papadimitriou, K. Steiglitz, Combinatorial Optimization: Algorithms and Complexity, Courier Corporation, 1982.

[34] L. Kaufman, P. Rousseeuw, Clustering by Means of Medoids, North-Holland, 1987.

[35] J. Friedman, T. Hastie, R. Tibshirani, The Elements of Statistical Learning, Vol. 1, Springer Series in Statistics, 2001.

[36] A. P. Dempster, N. M. Laird, D. B. Rubin, Maximum likelihood from incomplete data via the em algorithm, Journal of the Royal Statistical Society. Series B (Methodological) (1977) 1–38.

[37] L. Kaufman, P. J. Rousseeuw, Finding Groups in Data: An Introduction to Cluster Analysis, Vol. 344, John Wiley & Sons, 2009.